

Microstructural Characterization of the Shear Bands in Fe-Cr-Ni Single Crystal by EBSD

Huajie YANG¹⁾, J.H.Zhang¹⁾, Yongbo XU¹⁾† and Marc Andre' Meyers²⁾

1) Shenyang National Laboratory of Materials Sciences, Institute of Metal Research, Chinese Academy of Sciences, Shenyang 110016, China

2) University of California, San Diego, La Jolla, CA92093-0411, USA

[Manuscript received October 24, 2007, in revised form March 10, 2008]

An investigation has been made into the microstructural characterization of the shear bands generated under high-strain rate ($\approx 10^4 \text{ s}^{-1}$) deformation in Fe-15%Cr-15%Ni single crystal by EBSD-SEM (electron backscatter diffraction-scanning electron microscopy), TEM (transmission electron in microscopy) and HREM (high-resolution electron microscopy). The results reveal that the propagation of the shear band exhibits an asymmetrical behavior arising from inhomogeneous distribution in plasticity in the bands because of different resistance to the collapse in different crystallographic directions; The γ - ε - α' phase transformations may take place inside and outside the bands, and these martensitic phases currently nucleate at intersections either between the twins and deformation bands or between the twins and ε -sheet. Investigation by EBSD shows that recrystallization can occur in the bands with a grain size of an average of $0.2 \mu\text{m}$ in diameter. These nano-grains are proposed to attribute to the results of either dynamic or static recrystallization, which can be described by the rotational recrystallization mechanism. Calculation and analysis indicate that the strain rate inside the shear band can reach $2.50 \times 10^6 \text{ s}^{-1}$, which is higher, by two or three orders of magnitude, than that exerted dynamically on the specimen tested.

KEY WORDS: High-strain rate deformation; Adiabatic shear band; Electron backscatter diffraction (EBSD); Recrystallization; Fe-Cr-Ni single crystal

1. Introduction

Thermally-assisted localized shear is an important mode of deformation, leading to catastrophic failure of materials with low ductility. This phenomenon may occur frequently under high-strain rate deformation^[1-3], and also in quasi-static deformation in certain condition^[4]. For the former, shear localization is considered as adiabatic process, leading to a significant temperature rise in the shear bands, and in turn, decrease in the rate of work-hardening of materials. For the later case however, it is currently referred to as isothermal shear localization, implying that it is not related to thermal softening of materials, but controlled by dislocation planer slip^[5]. Shear localization arising from dynamic deformation is early recognizable in materials including ferrous metals, non-ferrous metals and polymers, and recent researches show that the similar deformation can occur frequently in metallic glasses in particular bulk metallic glasses^[6], and nanocrystalline metals are proven to have shear localization when deformed at low strain rates^[7,8].

Early observations of shear localization date back to Henri (1878)^[9] and to Harold Massey (1921)^[10], and later to Zener and Hollomon (1944)^[1]. However, extensive theoretical and experimental studies towards the improved understanding of shear localization have commenced around early seventies and intensified in the eighties. These efforts are involved mainly in both aspects of the theoretical description^[11-13] and the microstructural evolution^[14-19] of the shear bands. Although, a number of scientist in mechanics, materials and even physics have made a great efforts in understanding the mechanisms on shear band formation, there are some critical important problems such as

deformation structure, phase transformation and recrystallization and the transition from crystalline lattice to disordered structure in the bands, that have not been well understood so far. In this paper, we will present an investigation of the microstructural characteristics of localized shear deformation in a Fe-15%Cr-15%Ni single crystal deformed dynamically (strain rate: about 10^4 s^{-1}) by the collapse of an explosively driven thick-walled cylinder under prescribed initial temperature and strain conditions as part of general investigation on the structural aspects of the shear localization.

2. Material and Experimental Procedure

Single crystal of the Fe-15 wt pct Cr-15 wt pct Ni, which was grown at the Advanced Research and Development Laboratory at Pratt and Whitney Aircraft (West Palm Beach, FL), was chosen for this study. The alloy was homogenized at 1500 K for 72 h and has an FCC structure.

The generation for shear localization was generated by the thick-walled cylinder implosion technique introduced by Nesterenko *et al*^[20]. Scanning electron microscopy (SEM), transmission electron microscopy (TEM) and high-resolution electron microscopy (HREM) are commonly used to characterize the microstructural evolution of the shear bands, whereas few have been reported on studies of the microstructural evolution of the bands by EBSD (electron backscatter diffraction)^[19,21-23]. The fundamentals of the EBSD technique have been given in a review^[24]. Kikuchi patterns can be obtained automatically and the corresponding orientations of the grains and their boundaries can be detected by using orientation imaging microscopy (OIM) software. The angle resolution obtained by Kikuchi pattern can be improved to about

† Prof., to whom correspondence should be addressed, E-mail: ybxu@imr.ac.cn.

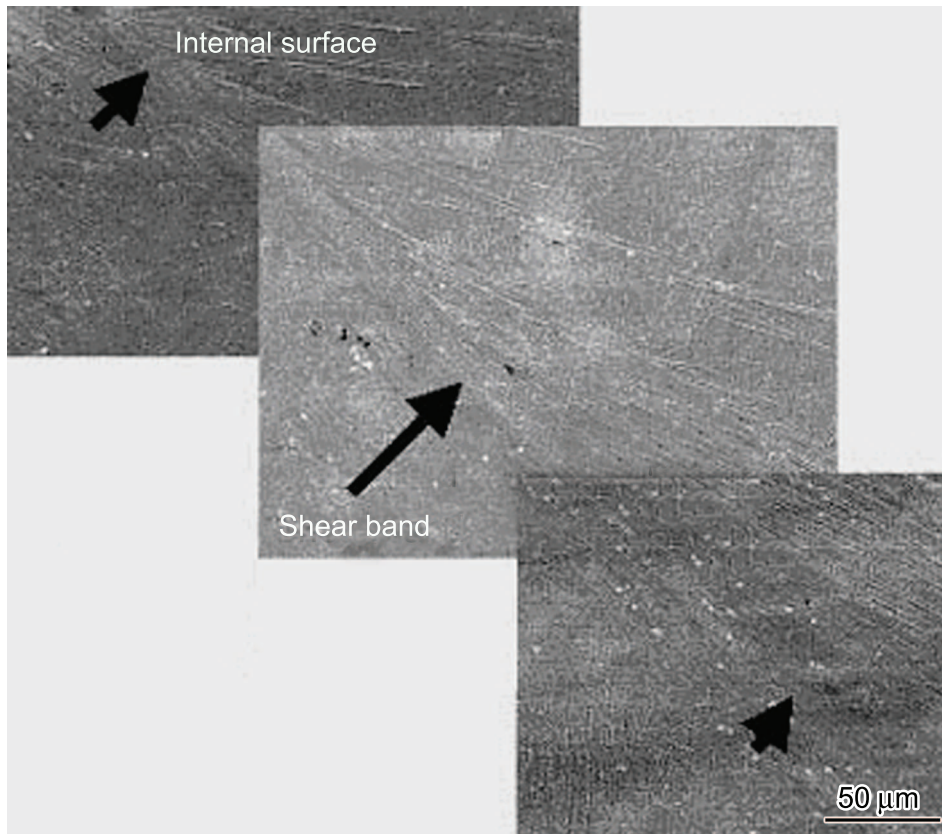


Fig.1 Axi-symmetrical distribution in plastic deformation of the shear band propagation in the Fe-Cr-Ni alloy monocrystal imaged by FESEM

1° when an field emission gun scanning electron microscopy (FEGSEM) with a small beam spot size is used. It should be mentioned that specimen preparation for EBSD investigation is critical and highly dependent on the material microstructure, in particular the surface conditions of the specimen because the EBSD signal usually comes from a few surface layer of atoms and deteriorates. Therefore, the specimens for EBSD were prepared by sectioning, followed by mechanical polishing and finally, electro-polishing carefully.

3. Results and Discussion

3.1 Morphology of shear localization

The collapse of thick-walled cylinder specimen is in a plane strain condition, and the stress state can be considered as a superposition of a hydrostatic pressure and a pure shear stress due to the axi-symmetrical geometry and loading. While the radial stress is zero at the internal surface, the tangential stress is maximum. The shear stress is the highest at the internal surface, and thus the shear bands preferentially occur at the internal surface as shown in Fig.1. Because the imploded force exerting on the internal surface of the specimen is not uniform, it will lead to the inhomogeneous in plastic deformation resulting in the distribution of the bands in length and space between the bands, and the number of the band from place to place^[25]. Xue *et al.*^[26] have proposed that this kind of characteristic distribution of the bands is geometrically neces-

sary due to the spiral trajectory of the bands, starting in the initial surface. As shown in Fig.1, the shear bands (marked by arrows) have a well defined boundary on one side, and are divergent (bifurcation) on the other side of the band. This kind of deformation phenomenon produced during band propagation is also observed in steels^[18] and Ti^[25]. It is proposed that the crystallographic anisotropy creates a mechanical anisotropy in the single crystal resulting in a difference in resistance to the collapse^[26]. Figure 2

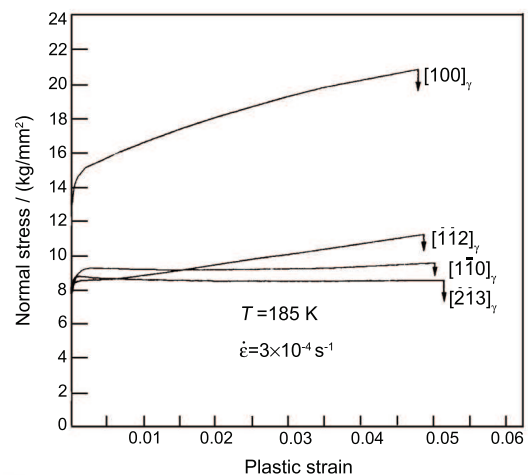


Fig.2 Stress-strain response for Fe-15%Cr-15%Ni single crystal along different directions of $[100]_\gamma$, $[1\bar{1}0]_\gamma$, $[\bar{1}\bar{1}2]_\gamma$ and $[\bar{2}\bar{1}3]_\gamma$ ^[27]

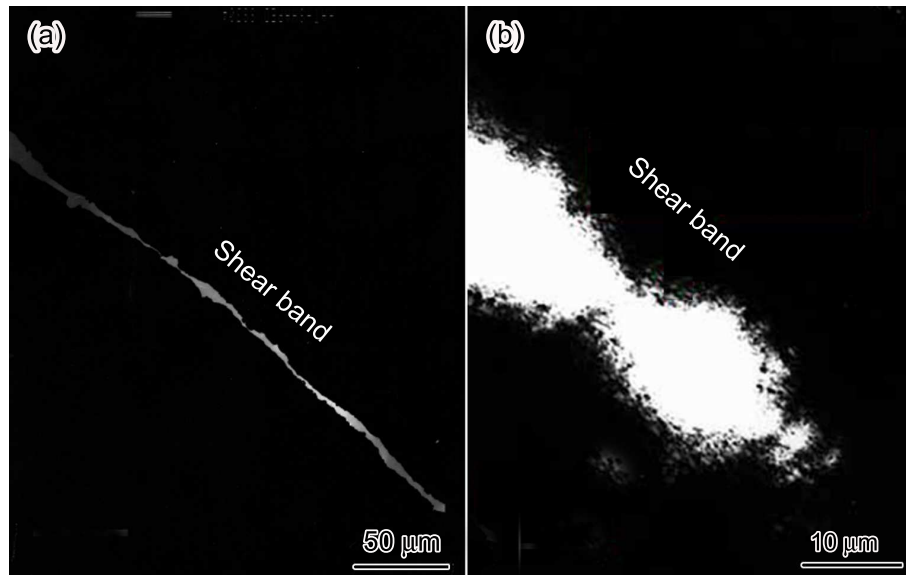


Fig.3 TEM images showing the low-magnification of a shear band produced during explosion (a), and the transparent perforated region around the band (b)

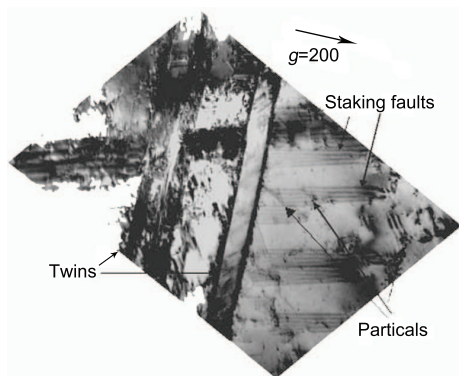


Fig.4 Twins, stacking faults and partial dislocations as well as stacking fault overlapping produced in the shear band during deformation localization

shows stress-strain response obtained by Stone and Thomas^[27] for different directions of $[100]_{\gamma}$, $[\bar{1}\bar{1}0]_{\gamma}$, $[\bar{1}\bar{1}2]_{\gamma}$ and $[\bar{2}\bar{1}3]_{\gamma}$ in the Fe-Cr-Ni single crystal. Obviously, the $[100]$ orientation in this alloy has four slip systems with identical Schmid factors and therefore a higher yield stress. And thus, the $[100]$ direction shows a greater resistance to collapse. A number of experiments with the thick-walled cylinder revealed that the band distribution on the cross-section of the specimen is not in a random manner, but regular, and with a well established and self-organized pattern. Their trajectories were, in all cases, spiral^[26].

3.2 Deformation microstructure within the shear bands

The small width of the bands renders microscopic examination difficult. In particular, it is very hard to prepare the thin-foil for TEM examination because the perforation generated by using ordinary methods does not coincide with the band area. In order to thin the shear band exactly during preparation for TEM observation, a fixed dimpling method was performed on the sample in some cases^[28]. The image shown in

Fig.3(a) is a bright field image of a shear band at low-magnification containing a shear band, and Fig.3(b) is a magnified bright-field image taken from a field along the band in Fig.3(a). It can be seen that a transparent perforated region is around the band, and all TEM observations of the band are performed on this region. It is generally accepted that the tendency for the dislocation cross-slip is weakened, and the possibility of the pile-up of dislocations is strengthened with decreasing stacking fault energy in FCC metals. Therefore the dislocations may extend into two partial dislocations and there is a piece of stacking fault between them. Figure 4 is a typical field showing the details of the dislocation structures in the band produced under high strain rate loading. It is characterized by twins and faults as well as partial dislocations. The partial dislocations bordered at a stacking fault and appeared on a coherent twin boundary are shown. The single partial dislocation in fact, is a step with $1/3\langle 111 \rangle$ on the coherent twin boundary. Analysis shows that these dislocations are the partial dislocations with a Burgers vector of $\frac{1}{6}[\bar{1}\bar{1}2]$. In addition, it is interesting to find that the stacking faults may overlap each other during moving on the parallel slip planes (see Fig.4), and the intrinsic and extrinsic stacking faults are separated by the partial dislocations. Figure 5(a) and (b) show high-order twins, and serious distortion of these twins, respectively. In fact that twinning of a material subjected to high-strain rate loading is a continuous and dynamic multiplied process^[18], micro-twins are generated continuously within the primary and high-order twins, and therefore the twins are quite plentiful within the shear bands (Fig.5(c)), and also the matrix channels between the twins have high concentration of dislocations.

3.3 γ - ϵ - α' phase transformation under high strain rate

A number of investigation shows that the martensitic transformation is an important mode of deformation for austenitic stainless steel with low-

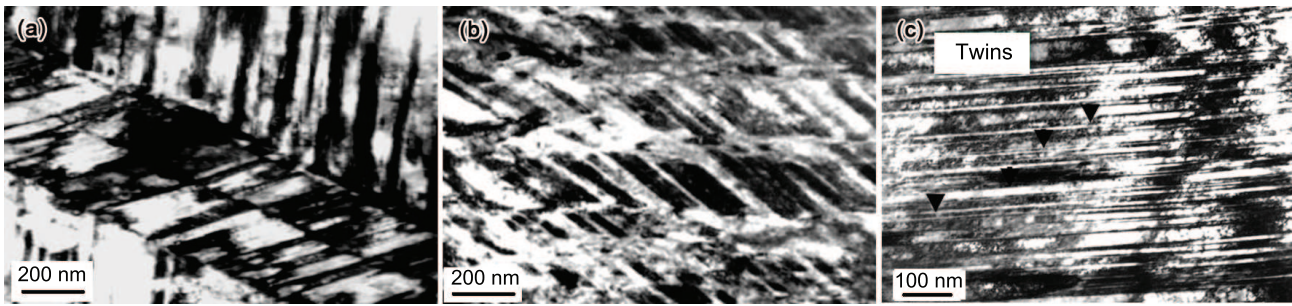


Fig.5 High-ordered twins (a), serious distortion of the twins (b), and plentiful twins in the band (c)

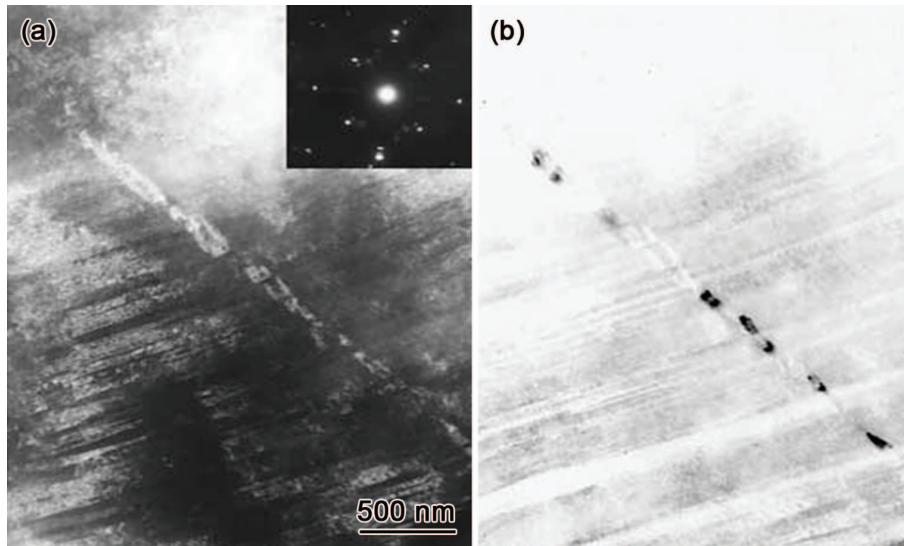


Fig.6 TEM bright-field (a), electron diffraction (insert), and dark-field images (b) showing α' -martensite phase transformation appears at the intersection between the twins and the shear bands in Fe-Cr-Ni monocystal subjected to explosive collapsed testing

stacking fault energy, in addition of dislocation glide and mechanical twinning. The transformation sequence when plastic strain is applied is $\gamma(\text{FCC}) \rightarrow \varepsilon(\text{HCP}) \rightarrow \alpha'(\text{BCC})$, which is further confirmed in the present work. Figure 6(a) shows a TEM bright-field image observed in the shear band in Fe-Cr-Ni monocystal under the cylindrical collapsed test with a strain rate of 10^4 s^{-1} , and its electron diffraction is also shown (insert). Figure 6(b) is the dark-field image of Fig.6(a). Analysis reveals that an α' -martensite phase transformation may take place in the shear band, and these phase transformation products have a certain crystallographic orientation relationship with their parent matrix. This kind of phase transformation particularly generates at the intersection between the shear band and twins. A similar α' -martensite phase transformation was also observed by Meyers *et al.*^[1] in 304 stainless steel, and they found that the crystallographic orientation relationship between the α' -martensite phases and the γ -austenite parent is in accordance with the Nishiyama orientation. Essentially, these results confirm earlier investigation made by Murr and Ross^[29], and Kestenbach and Meyers^[30] in tensile tests in the same materials. These α' -martensite laths nucleate preferentially at twin-band intersections where there are the sites for nucleation of the new phases^[31]. Figure 7(a) is a bright-field image taken from a filed

outside the bands, and the corresponding dark-field image taken by the diffraction spots from ε and α' -phases are shown in Fig.7(b) and (c), respectively, and the combined selected electron diffraction pattern is also shown (insert). Contrast analysis reveals that the ε -martensite and γ -parent have a certain crystallographic orientation relationship:

$$\{0001\}_{\varepsilon} // \{111\}_{\gamma}, \quad \langle 11\bar{2}0 \rangle_{\varepsilon} // \langle \bar{1}10 \rangle_{\gamma}$$

It is obvious from this analysis that the ε -phases form from stacking faults lying in the parent planes $(111)_{\gamma}$, the ε -martensite plane $(0001)_{\varepsilon}$ is parallel to $(111)_{\gamma}$. The intersection of the ε -bands and twins was found to be the preferred nucleation sites for the α' -phases as indicated in Fig.7, showing that the ε -sheets are the α' -phases embryos. It should be mentioned that a number of observations shows that the $\gamma \rightarrow \varepsilon$ transformation are not observed in the shear bands, but rather outside the bands. One possible reason for this is the higher rise in temperature in the shear bands. As the temperature in the bands increases, the stacking fault energy in austenite increases. Therefore, the ε -sheets are no longer stable relative to the austenite. This observation and analysis is in good agreement with those obtained in previous works^[32,33] and in recent research^[34]. Murr *et al.*^[35] have pointed out that

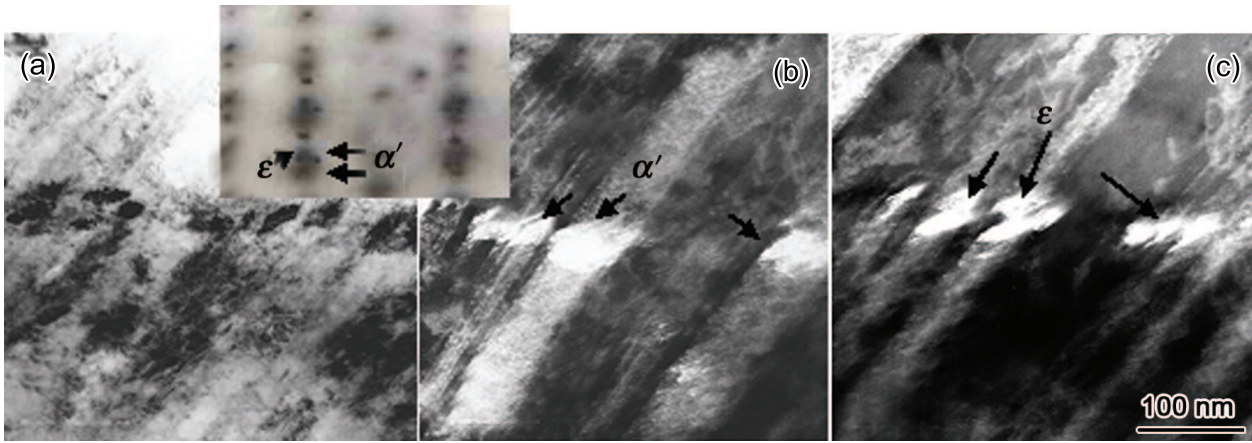


Fig.7 γ - ε - α' phase transformation occurring outside the shear band in Fe-Cr-Ni monocrystal subjected to explosive collapsed testing

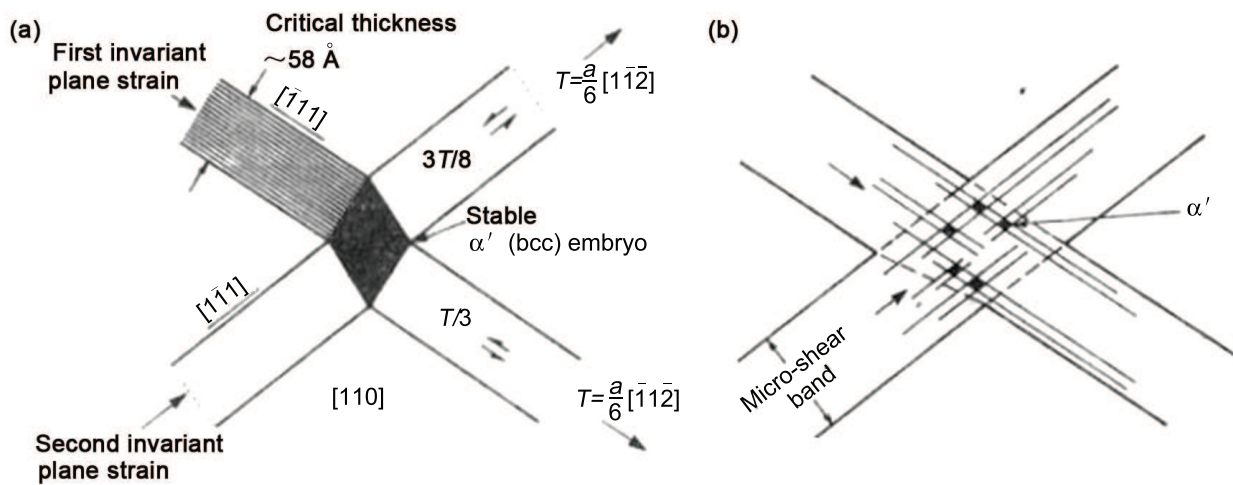


Fig.8 Schematic details of the α' (bcc) nucleation: (a) twin-fault displacements necessary for the nucleation of stable α' (bcc) embryos, and (b) the irregular formation of α' (bcc) embryos within a thick micro-shear band or twin-fault bundle^[35]

these two intersecting twin-fault bundles must have a specific defect or fault displacement structure as shown schematically in Fig.8(a). The requisite invariants, $3T/8$, where $T = \frac{a}{6} [1\bar{1}\bar{2}]$, and $T/3$, where $T = \frac{a}{6} [\bar{1}1\bar{2}]$, are recognized to be neither twins nor regular stacking faults or ε -phase. The condition can only be fulfilled irregularly within fault bundles, creating dispersed (heterogeneous) nuclei as shown in Fig.8(b). The α' (bcc) nucleation on $(111)_\gamma$ needs a defect with a width of 4–5 dislocations^[32], and the critical size for a nucleus is about 5–7 nm^[35].

3.4 EBSD characterization-recrystallization in the shear band

EBSD in a field emission SEM (FESEM) can allow a direct quantitative analysis of grains and subgrains as small as 0.2 μm , and gives accurate measurements of grain and subgrain size, detects texture and its correlation with grain or subgrain size, shape and position, and determines the distribution of boundary misorientation and type. Therefore, this technique was performed on both Fe-15%Cr-15%Ni monocrystal

and 304 stainless steel subjected to explosive collapse loading in order to further characterize the microstructure in particular recrystallization within the shear band. Figure 9 is the EBSD map shown in Euler contrast (Fig.9(a)) and in Kikuchi band contrast (Fig.9(b)), respectively. The scanning range covers an apparent shear band of 2 μm width with a well-defined interface on one side (top), and on the other side of the band (below). There is an apparent deformed region within which the substructures are highly bent and elongated towards the shear direction as a consequence of high-strain rate deformation. It should be noticed that the Kikuchi band contrast of the image in the shear band is blurred. The reasons are larger surface roughness and fine structures arising from the recrystallized grains with different orientation, leading to a low indexed rate. Figure 10 is a set of pole figures obtained in a region across the shear band (shown in Fig.9). It is shown that the orientation $\langle 100 \rangle$ of the red area outside the band is in good agreement with that of the starting single crystal orientation ($\langle 100 \rangle$). The substructures

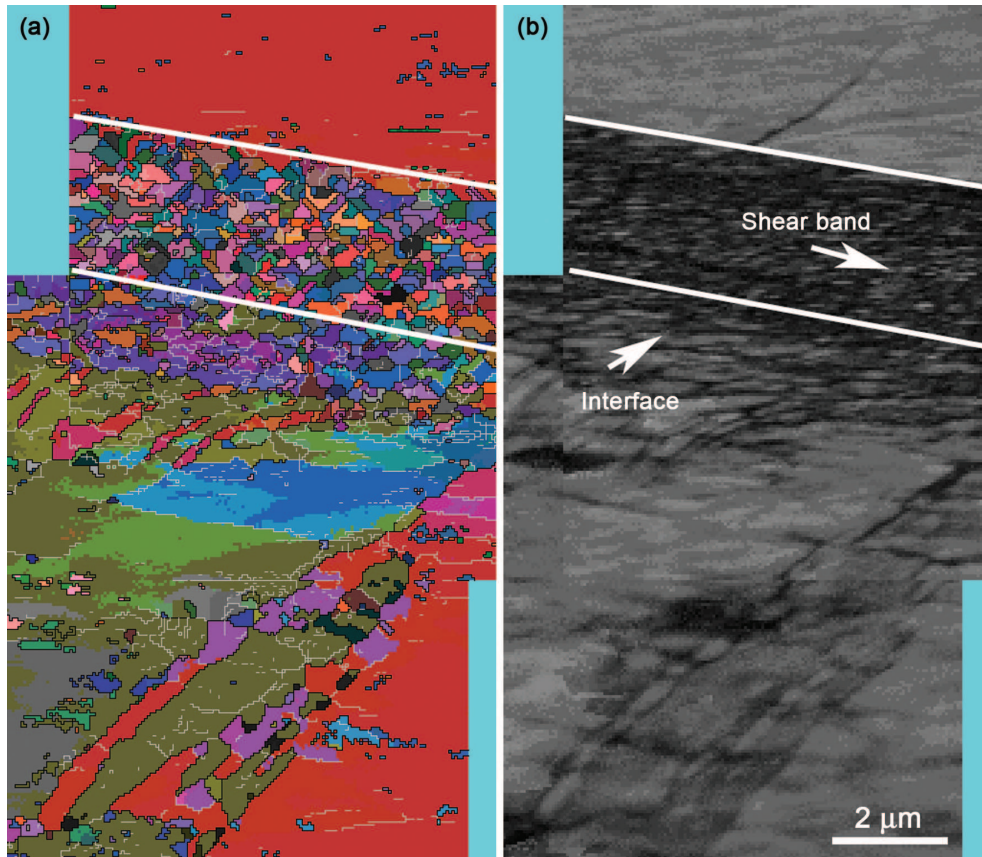


Fig.9 EBSD map of recrystallized grains in the shear bands in Fe-15%Cr-15%Ni monocrystal subjected to explosive collapsed loading, where the grains are shown in Euler contrast (a) and Kikuchi band contrast (b) (step size: $0.05 \mu\text{m}$; angle resolution: 1°)

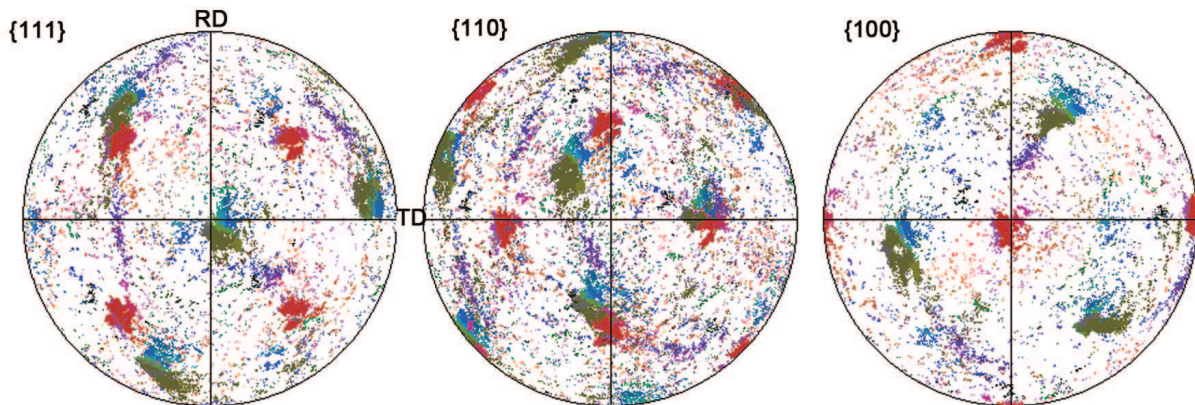


Fig.10 $\{111\}$, $\{110\}$ and $\{100\}$ pole figures showing the orientations across the shear band in Fe-15%Cr-15%Ni monocrystal

(colored in orange) below the shear band have an orientation of $\langle 111 \rangle$ parallel to ND, and the substructures (colored in blue) have a similar orientation of $\langle 111 \rangle$ parallel to ND. The misorientations between them (colored in orange and blue) are less than 5° . From Fig.9, one can see that the recrystallization occurs in the band and these new recrystallized grains are roughly equiaxed. The grain size distribution in the shear band is shown in Fig.11(a). It is clearly shown that most of the grains are smaller than 400 nm and the average size is about 200 nm in the shear band of this monocrystal. Boundary misori-

entations, which are readily obtainable from EBSD, enable the distribution of grain boundary type to be easily determined. Figure 11(b) shows the distribution of the grain boundary orientation in the shear band in Fe-Cr-Ni monocrystal. It is seen clearly that most grains in the band have high angle boundaries (15° – 60°). It should be mentioned that there is a peak of a low-angle boundary (2° – 15°) in this distribution, and these low-angle boundaries are in between the elongated substructures as seen in Fig.9, where the EBSD orientation map consists of three regions: a recrystallized grain region in the band, an elongated

substructure region towards the shear direction due to heavily deformation, and the monocrystal regions on both sides of the band, which are deformed slightly. It is reasonable to propose that substructures in the region adjacent to the shear band developed during high-strain rate deformation are those evolved from the structures in the band before recrystallization. It is surprising to find that a similar microstructure of shear band in 304 stainless steel, which is shown in Euler contrast (Fig.12(a)) and Kikuchi band contrast (Fig.12(b)). From these observations, one can see that whether in Fe-15%Cr-15%Ni monocrystal or 304 stainless steel, the grains in the bands are basically equiaxed implying that these new recrystallized grains form after deformation, rather than during or after localization. Wherever, recent observation shows that another mechanism of recrystallization in the band operates under the same test and the same material. This is shown in Fig.13, where the grains in the bands are shown in Euler contrast (a) and Kikuchi band contrast (b). In comparison of Fig.13 with Fig.9 and Fig.12, it can be found immediately that the grains in the bands shown in Fig.13 are not equiaxed, but elongated along the shear direction (indicated by arrow) with a long/shirt axis ratio of about 1.6. This implies strongly that these new recrystallized grains in the bands may occur during localization or not after deformation. In other words, they underwent shear deformation along the shear direction after localization. This is a strong evidence for dynamic recrystallization. It is known that the presence of the recrystallized grains in the shear bands has been reported in many studies in steel^[17,35] and other materials^[36-39] under

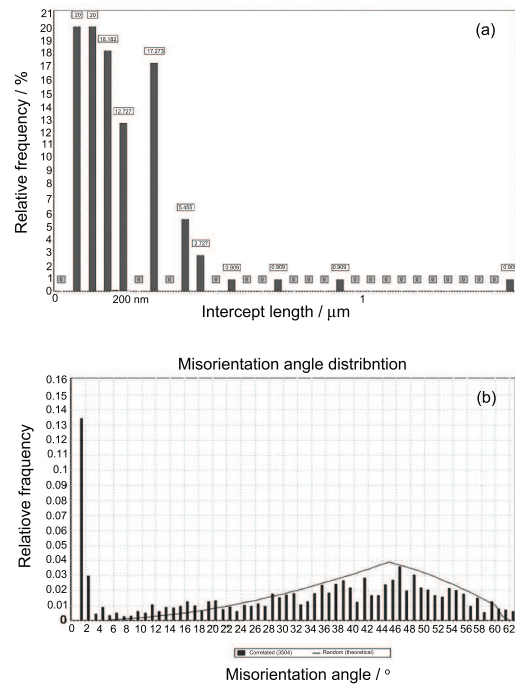


Fig.11 Distribution of the grain sizes (a) and grain boundary misorientation (b) in the shear band in Fe-Cr-Ni monocrystal (grain size was measured by linear intercept method)

high-strain-rate, but it has not been clear for a long time that whether the recrystallization microstructure develops simultaneously with localization (dynamic recrystallization) or subsequent to deformation

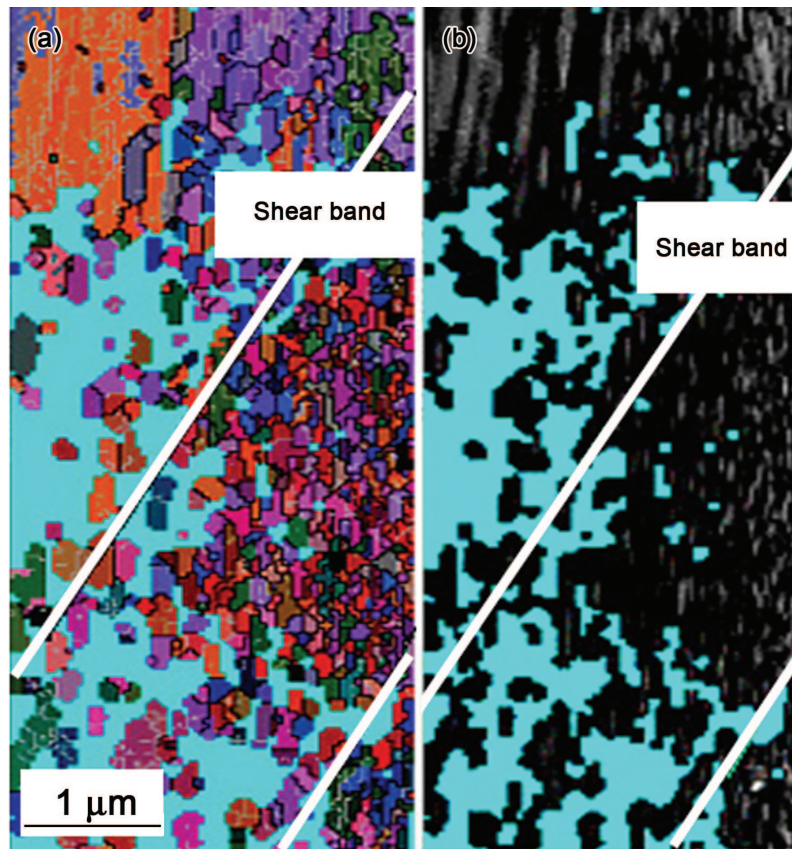


Fig.12 EBSD maps of recrystallized grains in the shear bands in 304 stainless steel subjected to explosive collapsed loading: (a) Euler contrast and (b) Kikuchi band contrast (step size: 0.05 μm, grain boundary black: >15°; silver: 2°-15°)

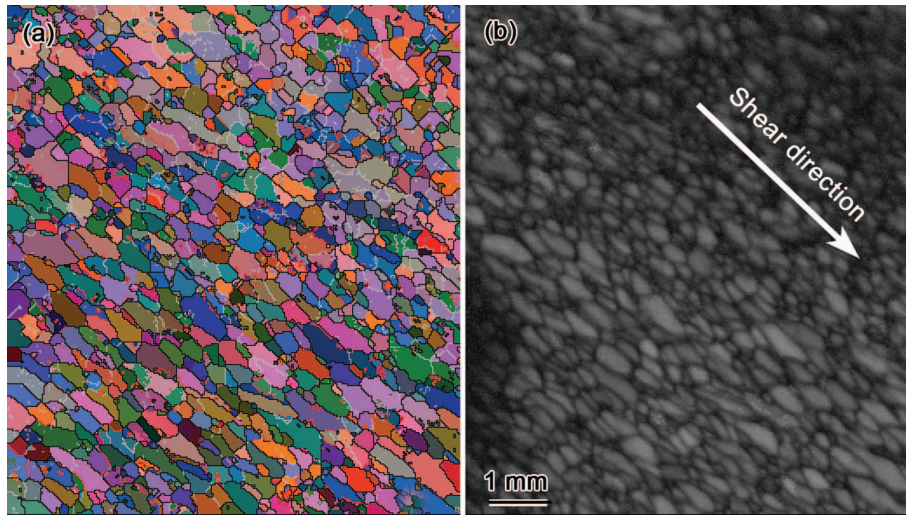


Fig.13 EBSD maps of recrystallized grains in the bands in Fe-15%Cr-15%Ni monocystal subjected to explosive collapsed loading: (a) Euler contrast and Kikuchi band contrast (b) (step size: $0.03 \mu\text{m}$, grain boundary: black: $>15^\circ$; silver: $2^\circ-15^\circ$)

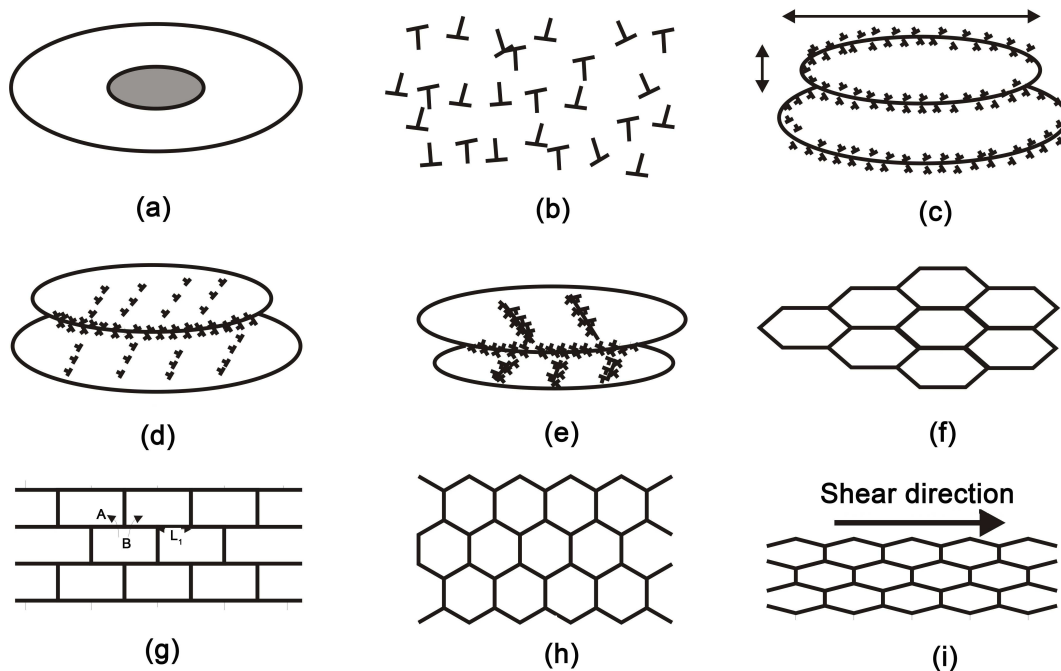


Fig.14 Schematic illustration of microstructural evolution and recrystallization in the shear band induced during high-strain rate loading in Fe-15%Cr-15%Ni monocystal: (a) single crystal before dynamic loading; (b) homogeneous dislocation distribution; (c) elongated substructure; (d) dislocation accumulation in substructure boundaries; (e) break-up of elongated substructures; (f) reorientation of sub-boundaries; (g and h) increase in orientation difference at boundaries and then rotation of sub-boundaries and formation of recrystallized grains with high angle boundaries, or (i) the newly recrystallized grain elongation along shear direction

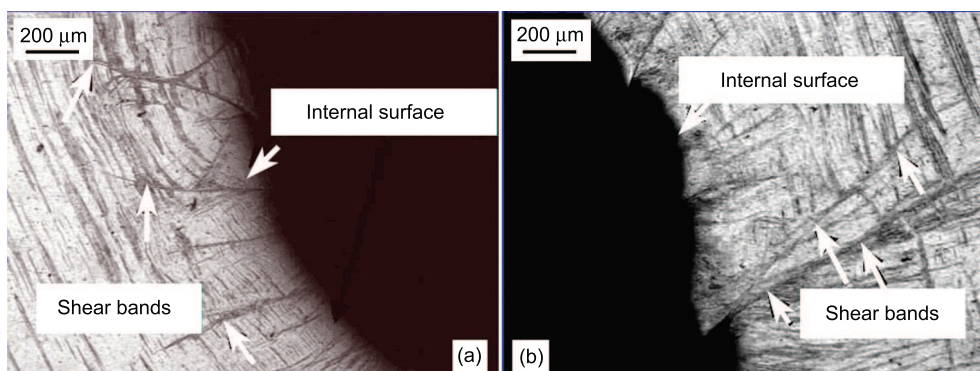


Fig.15 Shear bands initiating at the internal surface leaving some steps on them

(static recrystallization)^[40]. It is evident from the present study that the new recrystallization structure may occur either during localization or after localization. Derby^[41] has proposed two-type mechanisms (migration and rotation) describing the DRX (dynamic recrystallization). Because the time required for formation of the shear band is lower, by several orders of magnitude, to the time required to create new grains of the 0.1 μm size by the migration of the boundaries, conventional migrational recrystallization could not be considered to be the mechanism of DRX. However a number of investigations show that a variety of dislocation sources, including Frank-Read source, will be activated, and therefore dislocations are multiplied significantly under high-strain rate loading. Campbell *et al.*^[42] have pointed out that a typical Frank-Read source will begin to multiply in about 10×10^{-10} s and at that time the estimated plastic strain in a typical metal will be only 0.002. These dislocations will form the substructures such as cells and tangles, leading to heterogeneous distribution in microstrain in the shear bands while the temperature increases simultaneously. From the results observed by EBSD mentioned above, it is reasonable to propose that the elongated substructures observed in the interfacial region adjacent to the shear band, in fact, are the structures before recrystallization in the band. Therefore, it is expected that before recrystallization in the band as a consequence of dynamic deformation, the substructures are formed in the band and they are elongated and then rotated along the shear direction as the first step of the DRX (Fig.14(c-f)). And then a great number of dislocation are absorbed by the sub-boundaries, leading to an increase in orientation difference of the sub-boundaries. When the dislocation accumulation in the elongated sub-boundaries reaches a critical extent, these substructures will be developed into the mobile boundaries with high-angle boundary as nuclei for DRX (Fig.14(g)). After then, these nuclei of the new recrystallized grains will grow under the driving force associated with high-strain rate deformation and temperature increasing, and finally appear to be the equiaxed grains in the bands as shown in Fig.9(a), Fig.12(a) and also shown schematically in Fig.14(h), which is called static recrystallization. These new recrystallized grains after nucleation may develop simultaneously with shear deformation, and finally they are elongated along the shear direction, schematically shown in Fig.14(i), which is referred to as the dynamic recrystallization. This model is, as shown in Fig.14 schematically, in fact, in good agreement with those proposed independently by Meyers *et al.*^[17,19] and Li *et al.*^[43].

3.5 Super-high strain rate deformation in the bands

It is well known that once localized shear deformation has commenced, steep strain and strain rate as well as temperature rise will appear in the shear bands. It is shown clearly from Fig.15 that the shear bands initiate at the internal surface of the cylinder, and left a series of shear steps. The height of the step in the inner surface provides a displacement, and this displacement, divided by the width of the bands, gives the shear strain in the bands produced during dynamic loading. Routinely, the average shear strain is 30, and the average width of the shear band is 12 μm

based on the measurement of the present study shown in Fig.3. According to the equation proposed by Dodd and Bai^[44], the half-width of the shear band is expressed as follows:

$$\delta = \sqrt{\frac{\lambda \theta_*}{\tau_* \dot{\gamma}_*}} \quad (1)$$

the temperature rise within the bands obtained by assuming that 90% of deformation work is converted into heat:

$$\theta_* = \frac{0.9 \tau_* \dot{\gamma}_*}{\rho \cdot C} \quad (2)$$

The time required for shear band formation can be obtained by the following equation from the Eq.(1) with Eq.(2):

$$t = \gamma_* / \dot{\gamma}_* = \frac{\rho C}{0.9 \lambda} \delta^2 \quad (3)$$

where τ_* , $\dot{\gamma}_*$, γ_* are the shear stress, strain rate and shear strain rate, θ_* is the temperature rise in the band, λ is the coefficient of the heat conduction, ρ is the material density, C is the heat capacity. The parameters used in Eq.(3) are: $\rho=8.7 \text{ g}\cdot\text{cm}^{-3}$, $C=500 \text{ J}\cdot\text{kg}^{-1}\cdot\text{K}^{-1}$, $\lambda=14.7 \text{ W}\cdot\text{m}^{-1}\cdot\text{K}^{-1}$ for stainless steel, where the unit of t is μs , and the unit of δ is μm . From Eq.(3), it is found that the time required for formation of the band is 5.0 μs , and therefore, strain rate that the shear band underwent is $2.5 \times 10^6 \text{ s}^{-1}$, which is much higher, by two orders of magnitude, than that average strain rate (about 10^4 s^{-1}) exerted dynamically on the specimen, implying that formation of the shear band may accompany an abrupt increase in strain rate. In other words, the materials within the band underwent a super-high-strain rate deformation during localization. This is in good agreement with the experimental result in the investigation of Al-Li alloy obtained by Xu *et al.*^[45]. They have determined strain rate within the band, and found that the local strain in the band is 10.0, and localized time for band formation is equal to about 100 μs , and then the strain rate within the band is about $10 \times 10^5 \text{ s}^{-1}$, which is much higher than that of the average strain rate ($2.6 \times 10^3 \text{ s}^{-1}$) required for the formation of the shear bands. Giovanola^[46] measured directly shear strain rate in the shear band as a function of time in VAR 4340 steel by using a high-speed photography technique, and found that shear localization occurs in two sequential stages, and during the first localization, the strain rate (10^4 s^{-1}) jumps by more than an order of magnitude to values larger than 10^5 s^{-1} , then approaching $1.4 \times 10^6 \text{ s}^{-1}$ during second localization. Such very high strain and strain rate produced during localization in the bands have also been reported previously^[47]. A number of investigations show that a polycrystalline material with high strain rate sensitivity will appear to be deformed at a mode of super-plastic flow^[48-50]. Firstly, the structures in the shear bands are very fine; secondly, the temperature in the bands may raise, and even higher than melting temperature. All these provide the conditions for super-plastic deformation of the materials in the bands. Ashby and Verrall^[49] have proposed a constitutive equation to describe super-plastic flow of a material under high strain rate. They suggested that

when polycrystalline matter is deformed at temperature above $0.4T_m$, one possible mode of super plastic flow is a “diffusion-accommodated flow”. Dodd and Bai^[47] have pointed out that in the process of machining, although the average strain rate may be quite low, the strain rate in these narrow bands of shear may be markedly higher. Murr *et al.*^[50] have also suggested that the shearing deformation actually achieved inside the adiabatic shear band is extremely large; with shear strains as large as 10, and the mechanism to achieve this large strain involves DRX and superplastic flow by sliding of submicron, equiaxed recrystallized grains.

4. Conclusions

(1) Distribution of the shear bands produced dynamically under high-strain rate (about 10^4 s^{-1}) at ambient temperature by the collapse of an explosively driven thick-walled cylinder in a Fe-Cr-Ni monocrystal is inhomogeneous. This is proposed to arise from the crystallographic anisotropy leading to the different resistance to the collapse.

(2) The phase transformation of $\gamma(\text{FCC}) \rightarrow \alpha'(\text{BCC})$ in the shear bands and the $\gamma(\text{FCC}) \rightarrow \varepsilon(\text{HCP}) \rightarrow \alpha'(\text{BCC})$ out of the band in the Fe-Cr-Ni monocrystal were observed. These phase transformation products may have a certain crystallographic orientation relationship with their parent matrix.

(3) The nano-grains (about 200 nm) appearing in the shear bands are proposed to attribute to either the microstructure development during localization (dynamic recrystallization) or subsequent to deformation (static recrystallization).

(4) Calculation shows that the material within the shear bands undergoes a super-high strain rate deformation process, and strain rate inside the shear band may reach $2.50 \times 10^6 \text{ s}^{-1}$ which is higher, by two or three orders of magnitude, than that exerted dynamically.

REFERENCES

- [1] C.Zener and J.H.Hollomon: *J. Appl. Phys.*, 1944, **15**, 22.
- [2] H.C.Rogers: *Annu. Rev. Mater. Sci.*, 1979, **9**, 283.
- [3] A.Korbel, V.S.Raghunathan, D.Teirlinck, W.Spitzig, O.Richmond and J.D.Embury: *Acta Metall.*, 1984, **44**, 511.
- [4] Y.B.Xu, Z.G.Wang and Z.Q.Hu: *Metall. Trans.*, 1991, **22A**, 723.
- [5] Y.B.Xu: *J. Mater. Sci. Technol.*, 2007, **23**, 237.
- [6] J.J.Lewandowski and A.L.Greer: *Nat. Mater.*, 2006, **5**, 15.
- [7] D.Jia, K.T.Ramesh and E.Ma: *Acta Mater.*, 2003, **51**, 3495.
- [8] Q.Weil, L.Kecskes, K.T.Hartwing, K.T.Ramesh and E.Ma: *Acta Mater.*, 2004, **52**, 1859.
- [9] H.Tresca: *Proceeding of the Institute of Mechanical Engineers*, 1878, **30**, 301.
- [10] H.F.Massey: *Proceeding of Manchester Assoc Engineers*, Reprinted by the National Machinery Co, Tifon. OH, 1921, 190.
- [11] Y.L.Bai: *J. Mech. Phys. Solids*, 1982, **30**, 195.
- [12] T.G.Shawki: *Appl. Mech. Rev.*, 1992, **45**, S46.
- [13] R.C.Batra and Z.G.Wei: *Int. J. Impact Eng.*, 2007, **34**, 448.
- [14] Y.Me-Bar and D.Shechtman: *Mater. Sci. Eng.*, 1983, **58**, 181.
- [15] S.P.Timothy and I.M.Hutchings: *Mater. Sci. Technol.*, 1985, **1**, 526.
- [16] K.A.Hartley, J.Duffy and R.H.Hawley: *J. Mech. Phys. Solids*, 1987, **35**, 283.
- [17] M.A.Meyers, Y.B.Xu, Q.Xue, M.T.Perez-Prado and T.R.McNelly: *Acta Mater.*, 2003, **51**, 1307.
- [18] Q.Xue, E.K.Cerreta and G.T.Gray III: *Acta Mater.*, 2007, **55**, 691.
- [19] Y.B.Xu, J.H.Zhang, Y.L.Bai and M.A.Meyers: *Metall. Mater. Trans.*, 2008, **39**(4), 811.
- [20] V.F.Nesterenko and M.P.Bondar: *DYMAT J.*, 1994, **1**, 243.
- [21] V.F.Nesterenko, M.A.Meyers and T.W.Wright: *Acta Mater.*, 1998, **46**, 327.
- [22] M.T.Perez-Prado, J.A.Hines and K.S.Vecchio: *Acta Mater.*, 2001, **49**, 2905.
- [23] Q.Xue, J.F.Bingert, B.L.Henrie and G.T.Gray III: *Mater. Sci. Eng. A*, 2008, **473**, 279.
- [24] F.J.Humphreys: *J. Mater. Sci.*, 2001, **36**, 3833.
- [25] M.A.Meyers, B.Y.Cao, V.F.Nesterenko, J.D.Benson and Y.B.Xu: *Metall. Trans.*, 2004, **35A**, 2575.
- [26] Q.Xue, M.A.Meyers and V.F.Nesterenko: *Acta Mater.*, 2002, **50**, 575.
- [27] G.Stone and G.Thomas: *Metall. Trans.*, 1974, **5**, 2095.
- [28] K.P.Staudhammer, C.E.Frantz, S.S.Hecker and L.E.Murr: *Shock Waves and High-Strain-Rate Phenomena in Metals and Alloys*, Addison Dekker, 1981, 91.
- [29] L.E.Murr and M.F.Ross: *Phil. Mag.*, 1968, **18**, 281.
- [30] H.J.Kestenbach and M.A.Meyers: *Metall. Trans.*, 1976, **7A**, 1943.
- [31] G.B.Olson and M.Cohen: *Metall. Trans.*, 1976, **7A**, 1897.
- [32] W.S.Lee and C.F.Lin: *Scripta Mater.*, 2000, **43**, 777.
- [33] H.Fujita and S.Ueda: *Acta Metall.*, 1972, **20**, 5967.
- [34] C.X.Huang and S.D.Wu: *J. Mater. Res.*, 2007, **22**, 724.
- [35] L.E.Murr: *Metallurgical Effect of Shock and High-strain Rate Loading*, ed. by T.Z.Blazynski, Elsevier Applied Science, London and New York, 1987, 1.
- [36] M.C.Mataya, M.J.Carr and G.Krauss: *Metall. Trans.*, 1982, **13A**, 1263.
- [37] J.A.Hines, K.S.Vecchio and S.Ahzi: *Metall. Trans.*, 1998, **A29**, 191.
- [38] L.E.Murr, C.S.Niou and C.Fen: *Scripta Mater.*, 1994, **34**, 297.
- [39] V.F.Nesterenko, M.A.Meyers, J.C.Lasalvia, M.P.Bondar, Y.J.Chen and Y.L.Lukyanov: *Mater. Sci. Eng.*, 1997, **A229**, 23.
- [40] Y.B.Xu, Z.Ling and Y.L.Bai: *J. Mater. Sci. Technol.*, 2002, **18**, 504.
- [41] B.Derby: *Acta Mater.*, 1991, **39**, 955.
- [42] J.D.Campbell, J.A.Simmons and J.E.Dorn: *J. Appl. Mech.*, 1961, **28**, 447.
- [43] Q.Li, Y.B.Xu, Z.H.Lai, L.T.Shen and Y.L.Bai: *Mater. Sci. Eng.*, 2000, **A276**, 250.
- [44] B.Dodd and Y.L.Bai: *Mater. Sci. Eng.*, 1989, **5**, 557.
- [45] Y.B.Xu, W.L.Zhong, Y.J.Chen, L.T.Shen, Y.L.Bai and M.A.Meyers: *Mater. Sci. Eng.*, 2001, **A299**, 287.
- [46] J.H.Giovanola: *Mech. Mater.*, 1988, **7**, 59.
- [47] B.Dodd and Y.L.Bai: *Ductile Fracture and Ductility with Application to Metalworking*, Academic Press, London, 1987.
- [48] A.W.Weeber and H.Bakker: *Physica B*, 1988, **153**, 93.
- [49] M.F.Ashby and R.A.Verrall: *Acta Metall.*, 1973, **21**, 149.
- [50] L.E.Murr, E.A.Trillo, S.Pappu and C.Kennedy: *J. Mater. Sci.*, 2002, **37**, 3337.